Available online at www.sciencedirect.com

ScienceDirect

IFAC Papers Online CONFERENCE PAPER ARCHIVE

IFAC PapersOnLine 56-2 (2023) 6435–6440

Test Bed Emulation of Secondary Loop Refrigeration Units Using Peltier Elements: An Impedance Control Approach ⋆

Markus Fallmann * **Julian Kölbl** * **Tobias Ausweger** *
Maximilian Lösch * **Agnes Poks** * **Martin Kozek** *

* *TU Wien, Institute of Mechanics and Mechatronics, Getreidemarkt 9, 1060 Vienna, Austria (e-mail: markus.fallmann@tuwien.ac.at).*

Abstract: Advanced control methods help to increase the efficiency of refrigerated applications, easing their economic and ecological burden. However, approaches from literature have rarely been validated experimentally. One significant reason is the high expenses when conducting control experiments on full-sized plants. Low-maintenance, low-cost testing facilities constitute a possible remedy. Therefore, this work proposes a test bed refrigeration unit based on Peltier elements, for which impedance control compensates the behavioral differences to an actual secondary loop refrigeration unit. The two-degree-of-freedom control architecture comprises a static feedforward and a PID path that is robustified by choosing a linear design model based on the ν-gap metric. Experimental validation using a 260 min cycle shows that the achieved system trajectory lies within sensor accuracy to the desired one for more than 99% of the time, proving adequate emulation. Thus, the proposed concept is suitable to experimentally investigate high-level temperature control algorithms for refrigerated applications.

Keywords: Energy systems; Control system design; Robust control applications; Impedance control; Feedforward control; PID control

1. INTRODUCTION

Refrigerated transports use an enormous amount of energy, approximately 15% of the global fossil fuel, as reported by Adekomaya et al. (2016). Therefore, the economic and ecological savings potential of efficient refrigeration is apparent. Much has been done to improve hardware components, e.g., Glouannec et al. (2014) elaborated on wall insulation, and Artuso et al. (2020) on cooling unit design. Contrarily, control strategies have remained simple and almost unaltered for years.

Many proposed control strategies lack experimental validation. Since this weakened confidence in the practical applicability of postulated improvements, simple approaches still prevail in the industry. One reason for missing experimental validation is that conducting tests on a real plant is cost-intensive. As shown in the work of Fallmann et al. (2022), such experiments on an entire refrigerated truck require scrupulous maintenance and additional large-scale equipment like a climatic chamber to obtain conclusive statements. However, subordinate processes within refrigeration units are insignificant for investigating high-level control algorithms, for which nothing but the overall behavior is crucial. As remarked by Fasl (2013), especially secondary loop refrigeration units, with their additional flexibility, provide a research object promising in terms of efficiency increase by appropriate control. These demands highlight the need for a reliable, low-cost facility to verify high-level temperature control schemes experimentally.

Therefore, this work presents a low-cost test bed refrigeration unit based on Peltier elements. As it should act like a secondary loop refrigeration unit outlined by Wang et al. (2010), an impedance controller, according to Hogan (1984), imposes the desired dynamic behavior. The control design process relies on the ν-gap metric introduced by Vinnicombe (2000) to find a robust linear plant description suitable for parameter tuning. As recommended in Araki and Taguchi (2004), the feedforward path of the two-degree-of-freedom control architecture is then determined to meet reference specifications. Finally, experimental validation is presented.

The mathematical modeling of Peltier elements is well studied, and several authors estimated system parameters experimentally for such setups – see, e.g., Mannella et al. (2014). In the following, the same modeling approach is applied. Zhao and Tan (2014) summarized numerous applications of Peltier elements, indicating their versatile usability. Although utilized for refrigeration and air conditioning in general, the emulation of classic or secondary loop refrigeration units is not reported in literature. However, the industry's need for experimental proofs of concept and limited research budgets indicate the importance of downscaled but dynamically identical test beds for refrigeration applications. This work aims to close this gap.

⋆ This work was supported by the Austrian Research Promotion Agency (Forschungsförderungsgesellschaft) by the project *Industry4Redispatch* (grant number 887780).

10.1016/j.ifacol.2023.10.855

2. PROBLEM STATEMENT

The original refrigeration unit, i.e., the one to be emulated, exhibits a secondary loop setup, see Wang et al. (2010). Its classic cooling loop uses propane as a coolant, and a water-glycol mixture flowing through the storage loop serves as a single-phase cold reservoir, see Fig. 1a. Thereby, the cooling loop heat flow $\dot{Q}^{\mathrm{o}}_{\mathrm{cl}}$ decreases the storage temperature $\vartheta^{\mathrm{o}}_{\mathrm{s}}$, while the temperature of the air inside the cooling chamber, ϑ_{cc}, is directly affected only by the cooling chamber heat flow $\dot{Q}^{\mathrm{o}}_{\mathrm{cc}}$. In such a setup, a high-level controller for ϑ_{cc} has to determine the cooling unit switch s_{cu}, the compressor speed n_{cu}, and the fan switch s_{f}. Note that a superscript "o" labels inner quantities related to the original system.

Substituting the storage and cooling loop with an aluminum heat sink and a Peltier element yields a test bed refrigeration unit functionally similar to the original one, see Fig. 1b. According to the Peltier element's operating principle (see Zhao and Tan (2014) for detailed elaborations), a significant waste heat flow on the element's upper side accompanies the intended cooling loop heat flow $\dot{Q}_{\mathrm{cl}}$.

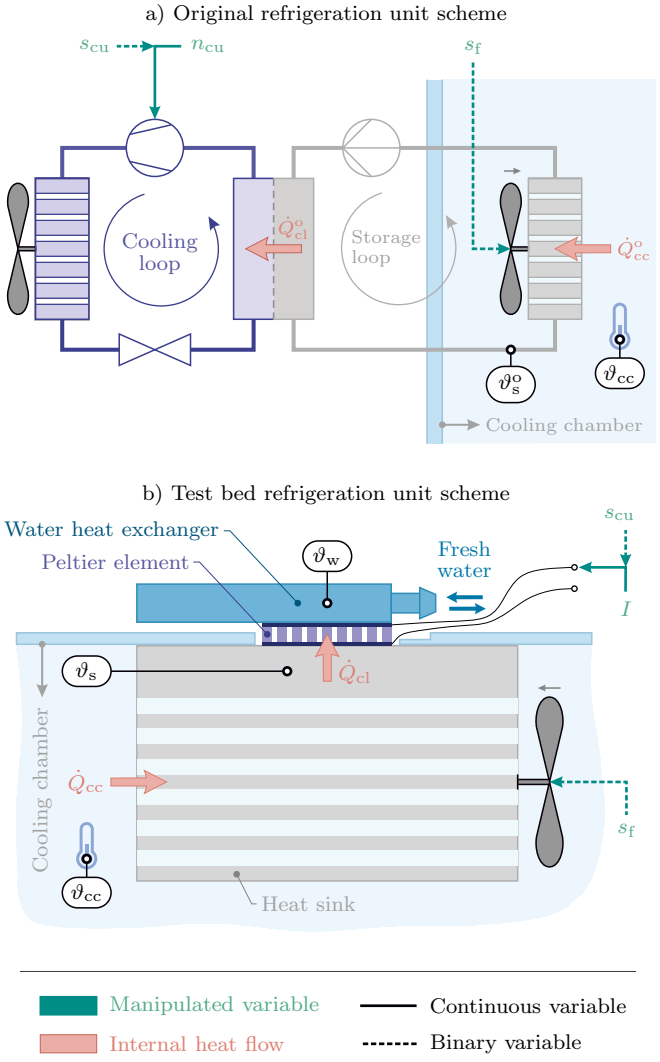

Fig. 1. Schematic illustration of (a) the original refrigeration unit and (b) its test bed counterpart.

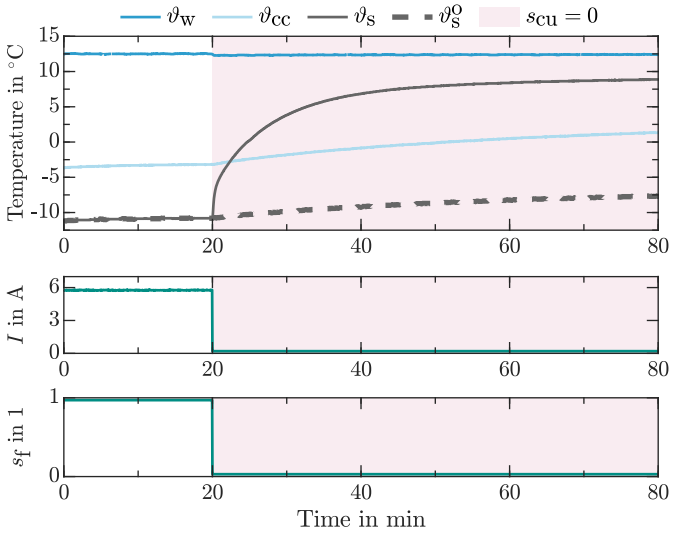

Fig. 2. Exemplary illustration of the differences between test bed system dynamics (storage temperature ϑ_{s}) and desired behavior, i.e., the evolution of storage temperature $\vartheta^{\mathrm{o}}_{\mathrm{s}}$, after turning off the cooling unit ($s_{\mathrm{cu}} = 0$). Here, $I = s_{\mathrm{cu}}\, I_{\mathrm{cu}}$ holds.

For this purpose, the mounted water heat exchanger is perfused with fresh water in sufficient amount so that the waste heat side temperature ϑ_{w} can be assumed constant.

Both setups depicted in Fig. 1 coincide regarding the manipulated inputs s_{cu} and s_{f}, and n_{cu} is replaced by the electrical current for cooling, I_{cu}, with which $I = s_{\mathrm{cu}}\, I_{\mathrm{cu}}$ holds. Therefore, a high-level ϑ_{cc}-controller has to determine s_{cu}, I_{cu}, and s_{f} in the test bed setup.

However, the main difference to the original system dynamic results from the Peltier element's thinness because the conductive heat flow based on the temperature difference between ϑ_{w} and ϑ_{s} significantly affects $\dot{Q}_{\mathrm{cl}}$, see Zhao and Tan (2014). If the cooling unit is active ($s_{\mathrm{cu}} = 1$), this conductive heat flow represents operational losses. On the contrary, if the cooling unit is switched off ($s_{\mathrm{cu}} = 0$), it severely compromises the dynamic analogy of the test bed by increasing ϑ_{s} significantly compared with how the storage temperature in the original system, $\vartheta^{\mathrm{o}}_{\mathrm{s}}$, would evolve, see Fig. 2.

Therefore, compensating for the undesired effect of occurring conductive heat losses remains the only open task to emulate the original system with the proposed test bed.

3. SYSTEM DESCRIPTION

The compensation task is more vividly apparent from the mathematical description of the test bed setup. In order to obtain a control-oriented model with lumped parameters, the storage dynamic is covered by a simple energy balance. It can be written in continuous time $t \in \mathbb{R}_{\geq 0}$ as

$$c_1 \frac{d}{dt}\vartheta_{\mathrm{s}}(t) = \dot{Q}_{\mathrm{cc}}(t) - \dot{Q}_{\mathrm{cl}}(t), \tag{1}$$

where $c_1 \in \mathbb{R}_{\geq 0}$ is the heat sink's heat capacity, $\vartheta_{\mathrm{s}} \in \mathbb{R}$ is the storage temperature, and $\dot{Q}_{\mathrm{cc}} \in \mathbb{R}$ and $\dot{Q}_{\mathrm{cl}} \in \mathbb{R}$ are the cooling chamber and cooling loop heat flows, respectively. The fan switch $s_{\mathrm{f}} \in \{0, 1\}$ determines whether the heat

transfer between the storage loop and the air inside the cooling chamber with temperature $\vartheta_{\mathrm{cc}} \in \mathbb{R}$ is driven by forced or natural convection. Thus, the associated heat flow can be modeled by

$$\begin{aligned}\dot{Q}_{\mathrm{cc}}(t) = c_{2,1}\,\left[\vartheta_{\mathrm{cc}}(t) - \vartheta_{\mathrm{s}}(t)\right]\,s_{\mathrm{f}}(t) + \dots \\ c_{2,2}\,\left[\vartheta_{\mathrm{cc}}(t) - \vartheta_{\mathrm{s}}(t)\right]\,\left[1 - s_{\mathrm{f}}(t)\right],\end{aligned} \tag{2}$$

where $c_{2,1} \in \mathbb{R}_{\geq 0}$ and $c_{2,2} \in \mathbb{R}_{\geq 0}$ are the heat transfer coefficients related to forced and natural convection, respectively. With the cooling unit switch $s_{\mathrm{cu}} \in \{0, 1\}$, the electrical current for cooling, $I_{\mathrm{cu}} \in \mathbb{R}_{\geq 0}$, and the compound current input $I = s_{\mathrm{cu}}\, I_{\mathrm{cu}}$, the Peltier element's cooling heat flow can be written according to Zhao and Tan (2014) as

$$\begin{aligned}-\dot{Q}_{\mathrm{cl}}(t) = \left[c_4\, I_{\mathrm{cu}}^2(t) - c_5\, I_{\mathrm{cu}}(t)\, T_{\mathrm{s}}(t)\right]\,s_{\mathrm{cu}}(t) + \dots \\ c_3\,\left[\vartheta_{\mathrm{w}} - \vartheta_{\mathrm{s}}(t)\right]\end{aligned} \tag{3}$$

with $T_{\mathrm{s}}(t) = \vartheta_{\mathrm{s}}(t) + 273.15$ for conversion from °C to K. Joule heating (coefficient $c_4 \in \mathbb{R}_{\geq 0}$) and Peltier effect (coefficient $c_5 \in \mathbb{R}_{\geq 0}$) only arise when the cooling unit is active, while heat conduction (coefficient $c_3 \in \mathbb{R}_{\geq 0}$) between the storage and the waste heat side with temperature $\vartheta_{\mathrm{w}} \in \mathbb{R}$ occurs permanently. In summary, the nonlinear hybrid model (1)-(3) covers the *actual* system dynamic – see Borrelli et al. (2017) for model classification.

Expressed in terms of model equations, the undesired effect of heat conduction described in Section 2 originates from the second line of (3) in case the cooling unit is inactive, i.e., $s_{\mathrm{cu}} = 0$. Hence, the *desired* system dynamic results as

$$\begin{aligned}c_1\,\frac{d}{dt}\vartheta_{\mathrm{s}}(t) = \dot{Q}_{\mathrm{cc}}(t) + \dots \\ \left[c_4\, I_{\mathrm{cu}}^2(t) - c_5\, I_{\mathrm{cu}}(t)\, T_{\mathrm{s}}(t)\right]\,s_{\mathrm{cu}}(t) + \dots \\ c_3\,\left[\vartheta_{\mathrm{w}} - \vartheta_{\mathrm{s}}(t)\right]\,s_{\mathrm{cu}}(t),\end{aligned} \tag{4}$$

where the factor s_{cu} in the third line is the only difference to the actual behavior (1)-(3).

Appropriate cooling in periods where $s_{\mathrm{cu}} = 0$ holds can balance these undesired conductive heat losses. Therefore, the applied input current is extended by the loss compensation current $I_{\mathrm{lc}} \in \mathbb{R}_{\geq 0}$ according to:

$$I(t) = s_{\mathrm{cu}}(t)\, I_{cu}(t) + \left[1 - s_{\mathrm{cu}}(t)\right]\,I_{\mathrm{lc}}(t) \tag{5}$$

Using (5) and a handy reformulation of (1)-(3), the *extended actual* system dynamic evolves to:

$$\begin{aligned}c_1\,\frac{d}{dt}\vartheta_{\mathrm{s}}(t) = \dot{Q}_{\mathrm{cc}}(t) + \dots \\ \left[c_4\, I_{\mathrm{cu}}^2(t) - c_5\, I_{\mathrm{cu}}(t)\, T_{\mathrm{s}}(t)\right]\,s_{\mathrm{cu}}(t) + \dots \\ c_3\,\left[\vartheta_{\mathrm{w}} - \vartheta_{\mathrm{s}}(t)\right]\,s_{\mathrm{cu}}(t) + \dots \\ c_3\,\left[\vartheta_{\mathrm{w}} - \vartheta_{\mathrm{s}}(t)\right]\,\left[1 - s_{\mathrm{cu}}(t)\right] + \dots \\ \left[c_4\, I_{\mathrm{lc}}^2(t) - c_5\, I_{\mathrm{lc}}(t)\, T_{\mathrm{s}}(t)\right]\,\left[1 - s_{\mathrm{cu}}(t)\right]\end{aligned} \tag{6}$$

One can see that it equals the desired behavior (4) if the last two lines vanish at all times. This means that the task of a loss compensation algorithm emerges to determine I_{lc} in a way to fulfill this condition. If satisfied, the test bed refrigeration unit (Fig. 1b) responds to a high-level controller's manipulated inputs s_{cu}, I_{cu}, and s_{f} like the original setup (Fig. 1a).

4. CONTROL STRATEGY

Based on (6), an ideal emulation results from a low-level controller that determines I_{lc} in a way that

$$c_3\,\left[\vartheta_{\mathrm{w}} - \vartheta_{\mathrm{s}}(t)\right] + \left[c_4\, I_{\mathrm{lc}}^2(t) - c_5\, I_{\mathrm{lc}}(t)\, T_{\mathrm{s}}(t)\right] = 0 \tag{7}$$

holds $\forall t \in \{t \,|\, s_{\mathrm{cu}}(t) = 0\}$.

A simple-minded approach immediately emerges: Directly applying I_{lc} according to the emulation condition (7) and the currently measured temperature ϑ_{s}. However, applying this control law drives the closed loop unstable.

A promising remedy to impose a certain dynamic behavior is impedance control, see Hogan (1984). For the specific task in this work, a mathematical description of the desired dynamic, i.e., the so-called impedance model, provides a storage temperature reference $\vartheta_{\mathrm{s}}^{\mathrm{ref}} \in \mathbb{R}$ based on current measurements. As shown in the overall control structure in Fig. 3, a subsequent two-degree-of-freedom (2DOF) controller then ensures asymptotic stability and accounts for sufficient control performance.

In the actual application, the electrical current is realized by a buck converter and a subordinate current controller. Due to their fast dynamics, their influence remains negligible, see Lösch (2022). Therefore, both dynamics are excluded from the investigation within this work.

4.1 Impedance model

Originating from the desired system dynamics (4) in case of loss compensation, i.e., $s_{\mathrm{cu}} = 0$, the reference temperature $\vartheta_{\mathrm{s}}^{\mathrm{ref}}$ results from solving

$$\begin{aligned}c_1\,\frac{d}{dt}\vartheta_{\mathrm{s}}^{\mathrm{ref}}(t) = \dot{Q}_{\mathrm{cc}}(t) \\ = c_{2,1}\,\left[\vartheta_{\mathrm{cc}}(t) - \vartheta_{\mathrm{s}}^{\mathrm{ref}}(t)\right]\,s_{\mathrm{f}}(t) + \dots \\ c_{2,2}\,\left[\vartheta_{\mathrm{cc}}(t) - \vartheta_{\mathrm{s}}^{\mathrm{ref}}(t)\right]\,\left[1 - s_{\mathrm{f}}(t)\right],\end{aligned} \tag{8}$$

for which the initial value $\vartheta_{\mathrm{s}}^{\mathrm{ref}}(t_0)$ is the measured storage temperature at t_0, the moment s_{cu} transitions from 1 to 0. Initialization is repeated at every such time t_0.

4.2 Temperature controller

The chosen 2DOF (Fig. 3) setup allows to tune the reference and disturbance behavior of the closed loop separately. As advised by Araki and Taguchi (2004), the PID path is parameterized to account for stability and disturbance specifications, while the feedforward path is subsequently designed to ensure satisfying reference tracking.

The PID path calculates the electrical current $I_{\mathrm{pid}} \in \mathbb{R}_{\geq 0}$ using the classic control law given by

$$I_{\mathrm{pid}}(t) = K_{\mathrm{p}}\,\left[e(t) + \frac{1}{T_{\mathrm{n}}}\,\int_0^t e(\tau)\,d\tau + T_{\mathrm{v}}\,\frac{de(t)}{dt}\right], \tag{9}$$

where $K_{\mathrm{p}} \in \mathbb{R}$, $T_{\mathrm{n}} \in \mathbb{R}_{\geq 0}$, and $T_{\mathrm{v}} \in \mathbb{R}_{\geq 0}$ denote the controller gain, integration time, and derivative time, respectively, and $e \in \mathbb{R}$ labels the control error given as:

$$e(t) = \vartheta_s^{ref}(t) - \vartheta_s(t) \tag{10}$$

Since the feedforward path will explicitly account for changes of ϑ_{cc} and s_{f}, only deviations from the optimal input current will remain as significant disturbances.

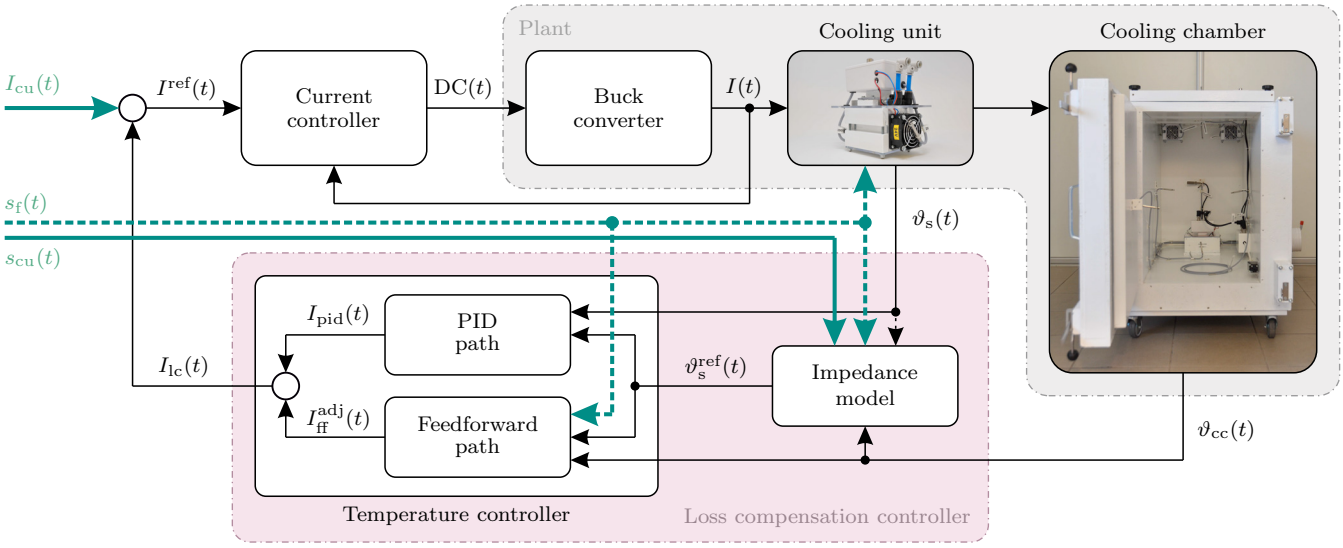

Fig. 3. Conceptual architecture of the overall control structure. The test bed plant comprises the cooling chamber, the cooling unit, and a buck converter for which a current controller determines the duty cycle DC to track a given current reference I^{ref}. Using system inputs and measured states, the temperature controller and the impedance model provide the electrical current I_{lc} to compensate for the undesired effect of occurring heat losses.

Therefore, rejection of such a disturbance current drives PID design. The nonlinear hybrid system dynamic (6) combined with its broad operating range calls for a robustly chosen linear tuning model. In this work, the ν-gap metric introduced by Vinnicombe (2000) was chosen for this purpose. It assesses the gap between two linear transfer functions in a closed-loop sense and quantifies the likelihood that one controller can achieve acceptable performance on both. This method is applied as follows: After linearizing (6) at a sufficiently high number of possible points within the operating range, the ν-gap is calculated for all combinations. Eventually, the linear model with the smallest gap to all others defines PID tuning. Here, specifications for disturbance rejection relate to a disturbance current of 1 A. The temperature overshoot should be lower than 0.25°C, and the control error should decay below 0.1°C within 75% of the system's time constant. PID parameters fulfilling these specifications are listed in Section 5.2.

To maintain simplicity, the feedforward path is implemented statically. The steady-state solution of (6) with $s_{cu} = 0$ and the replacement of I_{lc} and ϑ_s with I_{ff} and ϑ_s^{ref}, respectively, gives the feedforward current $I_{ff} \in \mathbb{R}_{\geq 0}$:

$$I_{ff}(t) = I_{ff}\left(\vartheta_s^{ref}(t), \vartheta_{cc}(t), s_f(t)\right) \tag{11}$$

Compared with a dynamic implementation, deviations from the optimal input current are expected due to its static character – see Lunze (2020). Improving reference performance and lowering PID workload, those deviations are reduced by an empirically determined adjustment factor $\alpha \in \mathbb{R}_{\geq 0}$, yielding the adjusted feedforward current $I_{ff}^{adj} \in \mathbb{R}_{\geq 0}$ as follows:

$$I_{ff}^{adj}(t) = \alpha(m) \cdot I_{ff}(t) \tag{12}$$

Due to the nonlinear hybrid system behavior, the performance depends on the particular mode transition m, i.e., how and when s_f transitions during active loss compensation ($s_{cu} = 0$). For the sake of brevity, the m-dependency of I_{ff}^{adj} is omitted. All transitions are depicted in Fig. 4, and corresponding coefficients are listed in Section 5.2.

In total, conductive loss compensation results from applying both paths according to

$$I_{lc}(t) = I_{pid}(t) + I_{ff}^{adj}(t) \tag{13}$$

Similar to (5), the reference $I^{ref} \in \mathbb{R}_{\geq 0}$ for the subordinate current controller is given by:

$$I^{ref}(t) = s_{cu}(t)\, I_{cu}(t) + [1 - s_{cu}(t)]\; I_{lc}(t) \tag{14}$$

To maintain clarity, stated binary factors are omitted in Fig. 3.

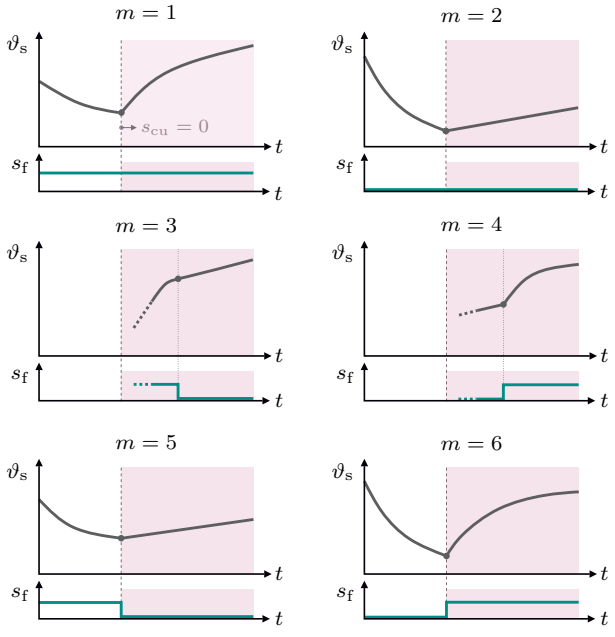

Fig. 4. Graphical illustration of the desired storage temperature evolution ϑ_s for all possible mode transitions m induced by combinations of the fan switch s_f and the cooling unit switch s_{cu}.

5. RESULTS AND DISCUSSION

5.1 Experimental setup

The proposed control strategy was implemented in a microcontroller in a discrete-time fashion and validated using a real-world testing facility. See Table 1 for setup specifications and Fig. 5 for the test bed cooling unit.

Table 1. Specifications of the setup

Condition	Value
Sampling time	2.5 s
Peltier element	ET-161-12-08-E
Heat sink	Fischer LA V 6-100-24
Fan	ebmpapst 614 NHH-119
Temperature sensor	Dallas DS18B20
Accuracy	±0.5 °C
Current Sensor	Texas Instruments INA260
Accuracy	±0.035 A

5.2 Parameterization

While used model parameters resulted from a comprehensive system identification carried out by Lösch (2022) for the same setup, methods described in Section 4 yield control parameters of PID and feedforward paths, see Table 2. Note that the controller gain K_p of the feedback structure shown in Fig. 3 is negative since a storage temperature higher than its reference demands further cooling.

Table 2. Model and control parameters

Parameter	(Estimated) value	Unit
ϑ_w	15	°C
c_1	530 (±0.3%)	J (°C)$^{-1}$
$c_{2,1}$	3.98 (±0.3%)	W (°C)$^{-1}$
$c_{2,2}$	0.30 (±0.5%)	W (°C)$^{-1}$
c_3	0.91 (±0.3%)	W (°C)$^{-1}$
c_4	1.14 (±0.1%)	W (A)$^{-2}$
c_5	0.06 (±0.2%)	W (A · K)$^{-1}$
K_p	−2	A (°C)$^{-1}$
T_n	20	s
T_v	0	s
$\alpha(1)$	0.75	1
$\alpha(2)$	2.25	1
$\alpha(3)$	1.50	1
$\alpha(4)$	0.20	1
$\alpha(5)$	2.75	1
$\alpha(6)$	0.55	1

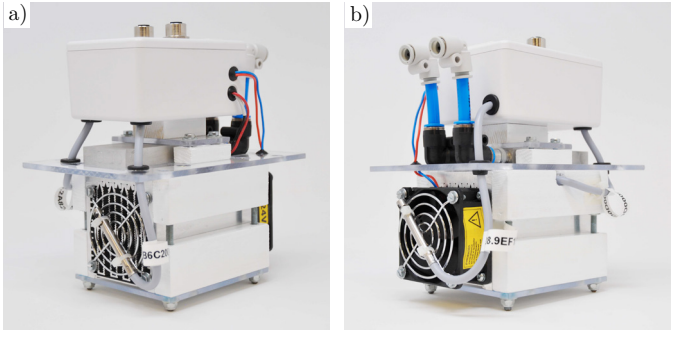

Fig. 5. Test bed cooling unit in diagonal (a) front and (b) rear view.

5.3 Control performance

The validation test cycle is 260 min long, and the inputs s_cu, I_cu, and s_f, which a high-level ϑ_cc-controller will determine in the eventual overall test bed, are chosen in a way to cover the usual operating range and all possible mode transitions, see Fig. 6. It is evident that the experimental setup fulfills the assumption of a constant temperature ϑ_w, postulated in Section 2. In periods of a turned-off refrigeration unit ($s_\mathrm{cu} = 0$), the loss compensation controller steps in to compensate for undesired conductive heat losses. The correspondingly applied current I_lc yields a good fit of the actual storage temperature ϑ_s to the desired behavior given by the reference $\vartheta_\mathrm{s}^\mathrm{ref}$.

A quantitative performance measure is given by the residual $r \in \mathbb{R}$:

$$r(t) = \vartheta_\mathrm{s}^\mathrm{ref}(t) - \vartheta_\mathrm{s}(t) \tag{15}$$

The second upper diagram of Fig. 6 shows its comparison to the temperature sensor's accuracy. On the one hand, more than 99% of the residuals are within this range (Fig. 7), and on the other hand, peaks occurring directly after mode transitions decay sufficiently fast. In general and compared with other works, e.g., Zhao and Tan (2014), the proposed algorithm performs satisfactorily.

Thus, the described test bed combined with the impedance-based loss compensation controller allows the emulation of a secondary loop refrigeration unit. Tests of high-level temperature controllers on such a test bed benefit from better plant reliability, reduced maintenance, and lower costs for the entire testing facility. Besides that, adapting the impedance model allows for emulating arbitrary dynamics, e.g., increasing the storage capacity. However, a dynamic feedforward path to get rid of empirical scaling factors and the explicit incorporation of the waste heat side temperature in case of insufficient fresh water supply seem beneficial to performance, highlighting promising areas for further research.

6. CONCLUSION

This work proposes a test bed setup based on Peltier elements to emulate secondary loop refrigeration units. Impedance control compensates deviations from the original system's behavior. A two-degree-of-freedom control architecture acts upon the nonlinear hybrid test bed, imposing the desired original system's dynamic. Experimental validation shows that the actual trajectory lies within the sensor accuracy to the desired one for more than 99% of the time. Thus, this concept constitutes a cost-efficient and reliable facility for higher-level testing, e.g., temperature control algorithms of entire cooling chambers. Furthermore, the impedance control scheme allows for simple changes in the desired behavior, further extending the test bed's applicability. Therefore, it enables building confidence in sophisticated control schemes that aim towards more efficient and environmental-friendly refrigeration.

ACKNOWLEDGEMENTS

The continuing support and assistance of Dennis Erdogan (TU Wien) and Michael Zauner (TU Wien) in real-world implementation issues is gratefully acknowledged.

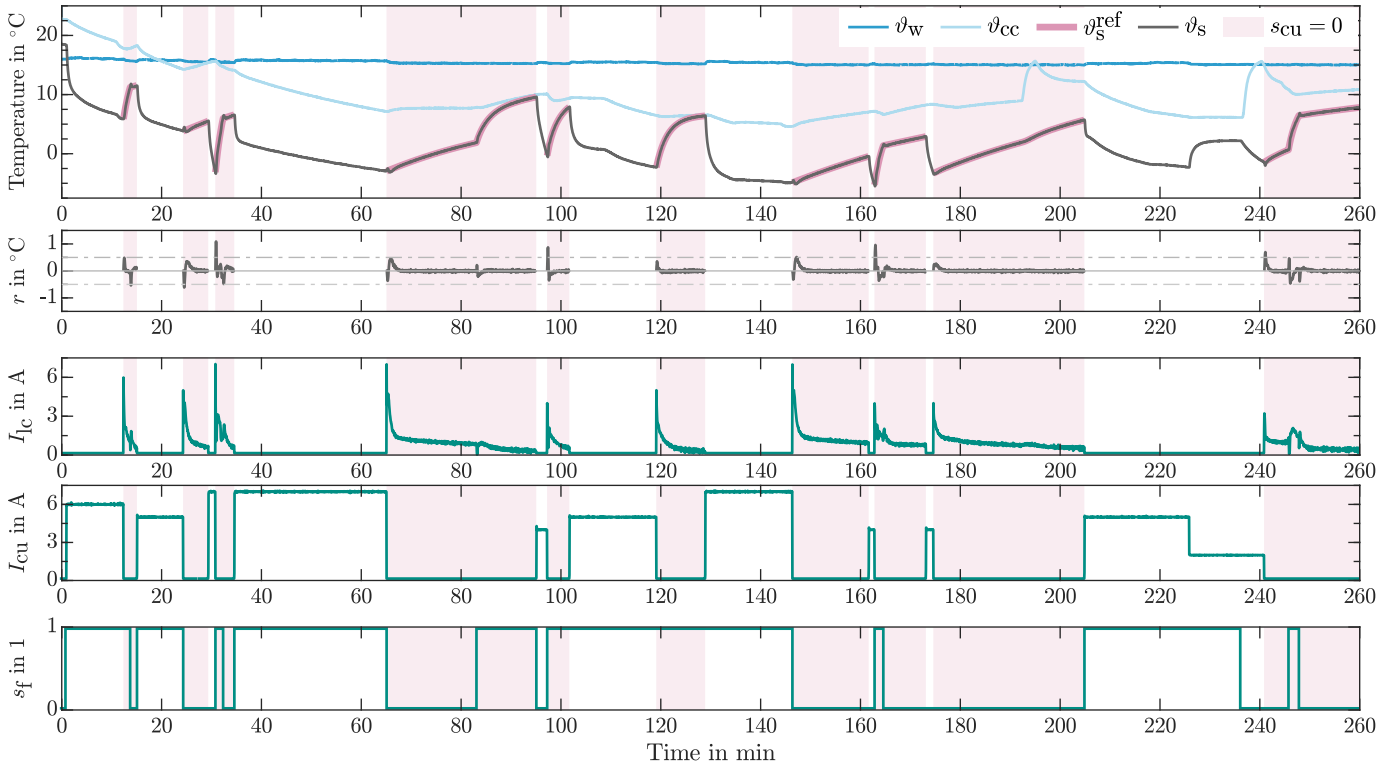

Fig. 6. Time-domain representation of experimental validation. The upper diagram shows measured temperatures ϑ_w, ϑ_{cc}, and ϑ_s, and the storage temperature reference ϑ_s^{ref} in periods when loss compensation is desired (background-shaded periods), i.e., when $s_{cu} = 0$ holds. Below are the residual (15), the loss compensation control action I_{lc}, and the predefined inputs I_{cu} and s_f.

REFERENCES

Adekomaya, O., Jamiru, T., Sadiku, R., and Huan, Z. (2016). Sustaining the shelf life of fresh food in cold chain – a burden on the environment. *Alexandria Engineering Journal*, 55(2), 1359–1365.

Araki, M. and Taguchi, H. (2004). Two-degree-of-freedom pid controller. *International Journal of Control, Automation, and Systems*, 1.

Artuso, P., Marinetti, S., Minetto, S., Col, D.D., and Rossetti, A. (2020). Modelling the performance of a new cooling unit for refrigerated transport using carbon dioxide as the refrigerant. *International Journal of Refrigeration*, 115, 158–171.

Borrelli, F., Bemporad, A., and Morari, M. (2017). *Predictive Control for Linear and Hybrid Systems*. Cambridge University Press.

Fallmann, M., Poks, A., and Kozek, M. (2022). Hybrid model-based online estimation of air temperature in mobile small-scale cooling chambers. *Applied Thermal Engineering*, 208, 118147.

Fasl, J. (2013). Modeling and control of hybrid vapor compression cycles. Master's thesis, University of Illinois at Urbana-Champaign.

Glouannec, P., Michel, B., Delamarre, G., and Grohens, Y. (2014). Experimental and numerical study of heat transfer across insulation wall of a refrigerated integral panel van. *Applied Thermal Engineering*, 73(1), 196–204.

Hogan, N. (1984). Impedance control: An approach to manipulation. In *1984 American Control Conference*, 304–313.

Lösch, M. (2022). Design, implementation, and experimental validation of a model predictive control scheme for refrigerated trucks. Master's thesis, TU Wien.

Lunze, J. (2020). *Regelungstechnik 1*. Springer Vieweg Berlin, Heidelberg.

Mannella, G.A., La Carrubba, V., and Brucato, V. (2014). Peltier cells as temperature control elements: Experimental characterization and modeling. *Applied Thermal Engineering*, 63(1), 234–245.

Vinnicombe, G. (2000). *Uncertainty and Feedback: H_∞ Loop-shaping and the ν-gap Metric*. Imperial College Press.

Wang, K., Eisele, M., Hwang, Y., and Radermacher, R. (2010). Review of secondary loop refrigeration systems. *International Journal of Refrigeration*, 33(2), 212–234.

Zhao, D. and Tan, G. (2014). A review of thermoelectric cooling: Materials, modeling and applications. *Applied Thermal Engineering*, 66(1), 15–24.

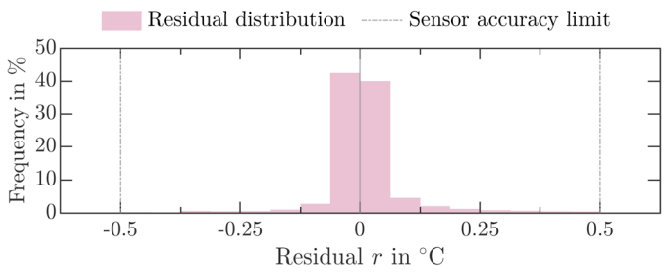

Fig. 7. Frequency distribution of the temperature residual (15) obtained from experimental validation.